SAND2019-13455J

Enhanced Self-Injection by Above Threshold Ionization Heating in a Laser Wakefield Accelerator

Y. Ma,[1,*] D. Seipt,[1] A. E. Hussein,[1] S. Hakimi,[2] N. F. Beier,[2] S. B. Hansen,[3] J. Hinojosa,[1] A. Maksimchuk,[1] J. Nees,[1] K. Krushelnick,[1] A. G. R. Thomas,[1] and F. Dollar[2]

[1] *Gérard Mourou Center for Ultrafast Optical Science, University of Michigan, Ann Arbor, Michigan 48109, USA*
[2] *Department of Physics and Astronomy, University of California, Irvine, California 92697, USA*
[3] *Sandia National Laboratories, Albuquerque, New Mexico 87185, USA*

We report on the experimental observation of a decreased self-injection threshold by using laser pulses with circular polarization in laser-wakefield acceleration experiments, compared to the usually employed linear polarization. A significantly higher electron beam charge was also observed for circular polarization compared to linear polarization over a wide range of parameters. Theoretical analysis and quasi-3D particle-in-cell simulations are in good agreement with the observed experimental findings and indicate a different injection path for circularly polarized laser pulses, originating from larger momentum gain during above threshold ionization. This enables electrons to fulfill the trapping condition more easily, and the resulting higher plasma temperature was confirmed via spectroscopy of the XUV plasma emission.

Laser-wakefield acceleration (LWFA) [1] has experienced a rapid development in the last four decades, now capable of generating high quality electron beams with multi-GeV energies [2–5]. Such high energy electron beams have the capability to drive novel secondary particle and radiation sources, such as positrons [6], bright X-rays [7], collimated γ-rays from inverse Compton scattering [8, 9] and even facilitating experimental strong-field quantum electrodynamics (QED) studies [10, 11]. It is also a promising source for compact X-ray free electron lasers (XFELs) [12]. However, these applications place highly restrictive requirements on the beam quality in terms of energy spread, emittance, beam charge, shot-to-shot stability and so on, especially for seeding XFELs [13, 14]. The electron beam quality critically rely on the control of the injection process and subsequent beam dynamics.

In LWFA, especially in the nonlinear "bubble" regime [15, 16], ambient electrons which are expelled outward transversely by the laser ponderomotive force slip backwards to the rear of the bubble and get trapped by the wake field if their longitudinal velocity becomes higher than the phase velocity of the plasma wave within the bubble. This is the so-called "self-injection" process. Due to the laser pulse evolution, and hence the plasma wave evolution, it is normally difficult to precisely control the self-injection process. Therefore, to lower the threshold of self-injection and to better control the trapping process, various injection schemes have been conceived [17–23].

Self-injection depends on a combination of the plasma density and laser intensity. It was recently studied extensively with parametric scans in particle-in-cell simulations [24]. Theoretical and numerical simulation studies have shown that the trapping threshold can be lowered by thermal effects in a warm plasma [24, 25], or in the self-modulated laser wakefield accelerator (SM-LWFA) regime via the coupling of Raman backscattering [26]. The latter indicates a polarization dependence to the trapping threshold. In LWFA in the bubble regime, the influence of laser polarization has rarely been considered because the dominating factor for the generation of laser wakefields is the ponderomotive force, which is polarization-independent. However, the dynamics of ionization with different laser polarization gives rise to considerable transverse and longitudinal momentum, which could facilitate the injection process [27–29].

In this letter, we investigate the role of laser polarization in electron self-trapping in LWFA with experiments and numerical simulations. We discovered that self-injected electron beams can be generated with a circularly polarized (CP) laser pulse at plasma densities 20% lower than the self-injection threshold for a linearly polarized (LP) laser pulse. When the laser power and plasma density is sufficient for self-injection in both cases, the total beam charge using CP laser pulses can be an order of magnitude higher than that with LP pulses. The enhancement of self-injection in the CP case is due to above threshold ionization heating in which electrons gain residual momenta due to the conservation of transverse canonical momentum while interacting with the laser pulse. After collisional relaxation, this results in a higher plasma temperature for CP, which was confirmed via XUV spectroscopy of the plasma emission.

The experiment was performed at the HERCULES laser facility at the Center for Ultrafast Optical Science (CUOS) at the University of Michigan [30]. The laser beam with an averaged power of $P_L = 50.4 \pm 3.2$ TW after compression was focused by an $f/20$ off-axis parabolic (OAP) focusing optic to a spot size of $w_0 = 26.0 \pm 0.8$ μm (at $1/e^2$ in intensity). The laser pulse duration is 35 ± 3 fs full-width-at-half-maximum (FWHM). The corresponding peak laser intensity is about 6.5×10^{18} W/cm^2, which gives a normalized laser intensity $a_0 = 1.8$ for the LP case, while a_0 is a factor of $\sqrt{2}$ smaller for CP at the same intensity. To switch between LP and CP, a 1/4 λ

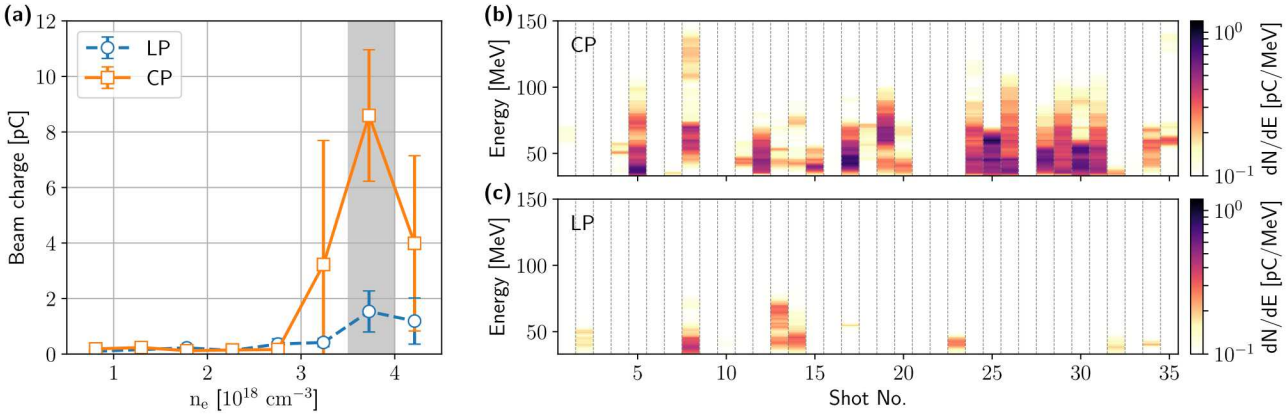

FIG. 1. (a) Electron beam charge as a function of plasma density with LP laser (blue circles) and CP laser (orange squares) with the same laser power of $P = (50.4 \pm 3.2)$ TW. The error bars represent the 2σ uncertainty. (b) and (c) Angularly integrated electron spectra of 35 consecutive shots at plasma density $n_e = (3.8 \pm 0.4) \times 10^{18}\text{cm}^{-3}$ (shaded region in (a)) for CP and LP, respectively.

mica wave plate of thickness 40 μm, was placed into the beam path before the OAP. By rotating the axis of the plate the polarization can be switched without affecting the laser intensity and focus quality.

The target was a 3D-printed variable-length gas-cell [31] filled with pure helium. A gas-cell suppresses plasma density ripples, which amplify self-injection in supersonic gas jets [32]. The plasma density was characterized using a Mach–Zehnder interferometer with a probe beam arriving at the target 20 ps after the main beam. The plasma density can be expressed as $n_e[10^{18}\text{cm}^{-3}] = 0.05 \times p_g[\text{psi}] - 0.16$, in the range $p_g \in [20, 120]$ psi backing pressure.

Electron energy spectra were measured using a dipole magnet (15 cm long, 0.8 T), a Lanex screen imaged onto a 12-bit CCD camera. The dispersion of the electron spectrometer was determined by a particle tracking code using the measured magnetic field [33]. To determine the electron beam charge, the Lanex signal was calibrated by using a Fuji BAS-MS image plate [34] which gives 2.9×10^{-6} pC/count [35]. A flat-field XUV-spectrometer [36] comprising a gold-coated diffraction grating and a 16-bit CCD was placed 3 m from the target to collect the on-axis plasma emission within a spectral range of $41 - 250$ eV. The resolving power of the spectrometer is approximately 1100 in the region of interest around 50 eV.

A comparison of the electron beam charge with LP and CP laser pulses as a function of plasma density at the same laser power is shown in Fig. 1(a). The self-injection threshold density is lowered from $3.2 \times 10^{18}\text{cm}^{-3}$ for LP to $2.7 \times 10^{18}\text{cm}^{-3}$ for CP. Consequently, the threshold ratio of laser power to critical power for self-guiding P/P_c is lowered from 5.5 for LP to 4.6 for CP, where $P_c[\text{GW}] = 17.4(n_c/n_p)$ [37], $n_c = m_e\epsilon_0\omega_0^2/e^2$ is the critical density for the laser angular frequency ω_0. These values are comparable with reported values in Ref. [38–40] for a LP laser. Fig. 1(b) and (c) show the electron spectra with CP and LP for a series of contiguous shots at plasma density of $n_e = (3.8 \pm 0.4) \times 10^{18}\text{cm}^{-3}$.

As shown in Fig. 1(c), the reproducibility with the LP laser is such that a beam was measured for approximately 10% of the laser shots, with an averaged beam charge of 1.54 ± 0.7 pC. Here, the relatively large error comes from the fact that the electron beam is absent in most of the shots in this case. With CP, as shown in Fig. 1(b), the reproducibility of the electron beam with energy higher than 50 MeV was increased to about 70% of shots having an electron beam, with an averaged beam charge of 8.6 ± 2.3 pC. Note that the effect is consistent over a range of densities, as indicated in Fig. 1(a). These experimental measurements indicate that the laser polarization has a significant effect on the trapping threshold.

To understand the experimental results, particle-in-cell (PIC) simulations were performed over a wide range in laser and plasma parameter space using the quasi-3D code FBPIC [42], which is numerical dispersion free. For most of the simulations runs, the simulation box with a moving window was of dimensions 50 μm $\times$ 80 μm with a resolution of $\Delta z = 0.04$ μm and $\Delta r = 0.27$ μm where z and r are the longitudinal and radial directions, respectively. Three azimuthal modes to resolve the departures from the cylindrical symmetry of the wakefield acceleration and 24 macro-particles in each grid cell were used. In these simulations, the laser pulse, either CP or LP, has a fixed FWHM pulse duration of 31 fs, while w_0 varies in the range $20 - 30$ μm and a_0 (LP) varies in the range $1.0 - 2.0$. The plasma is generated via field ionization of the pure neutral Helium target and the electrons originating from the two ionization levels are separately diagnosed. The helium density varies in the range of $(1.0 - 4.0) \times 10^{18}$ cm^{-3} for different simulation runs, while in each single run the density distribution is uni-

form with a 100 μm-long linear ramp before the arrival of the laser pulse. Benchmarking runs with higher spatial resolution, more particles-per-cell and larger numbers of azimuthal modes were performed to ensure convergence.

Fig. 2 shows the total charge of the injected electron beam in the PIC simulations over a parameter space of $(a_0,\ n_e)$. For almost all the simulation runs, the total beam charge with the CP laser is much higher than that with the LP laser, i.e., to obtain a certain amount of beam charge, the required laser power is lower for CP than LP, as we can see from the contour lines, which represent the beam charge at 0.1 pC, 10 pC and 100 pC for instance. If we treated the injection threshold as 1 pC, then P/P_c for CP and LP are 7.3 and 7.9, respectively. In general, the PIC simulations agree well with the experimental results; the self-injection threshold with the CP laser is lower than that with the LP laser and the total injected beam charge for CP with same laser intensity is higher than that with the LP laser. It is worth noting that more than 95% of the injected electrons come from the second ionization state for the CP case while only about 75% for the LP case.

The plasma wave excitation is nearly identical for CP and LP since it is driven by the ponderomotive force of the laser pulse, which is polarization independent. There are two pieces of evidence supporting this argument. First, the potential of the wakefield for CP and LP at the same time step is nearly identical. Second, the evolution of the peak laser intensity has an averaged difference of only 0.4% between the two cases. This indicates that the response of the laser pulse to the plasma

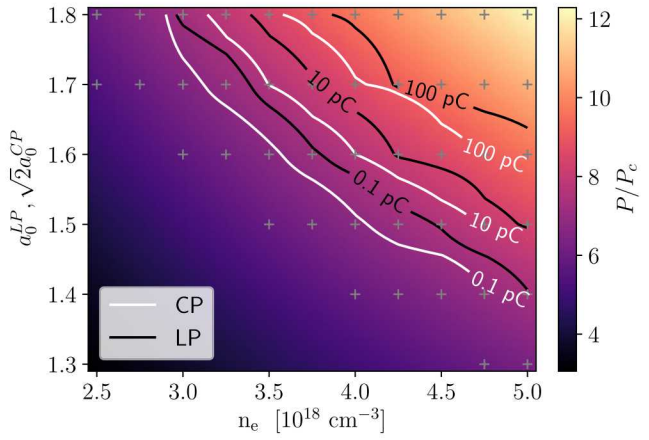

FIG. 2. Contour plots of injected beam charge from PIC simulations in a parameter space of (a_0, n_e) overlapped on P/P_c. For all simulation runs (gray crosses, each one for both CP and LP), the laser spot size is fixed at $w_0 = 26$ μm, all the other laser and plasma parameters as well as the simulation settings are the same. The best linear fits of P/P_c for the three example charge values, [0.1, 10, 100] pC, are [6.8, 7.8, 9.0] for CP and [7.4, 8.4, 9.7] for LP, respectively.

(and vice versa) is similar for CP and LP. Therefore, we might expect similar particle trajectories in the wake for CP and LP; the fact that both the experiments and simulations show such a dramatic difference in the trapped charge thus requires further explanation.

The reason for the difference is the momentum gain during the ionization process occurring prior to the peak pulse arrival. Ionization in a strong field proceeds via the *above threshold ionization* (ATI) mechanism [43] in which the ionized electrons gain kinetic energy in excess of the ionization potential (IP). After leaving the laser pulse, electrons gain residual transverse momentum $\mathbf{p}_\perp = m_e c\mathbf{a}_i$, where $\mathbf{a}_i = e\mathbf{A}_i/m_e c$ is the normalized laser vector potential at ionization, due to the conservation of transverse canonical momentum. This is accompanied by a longitudinal momentum gain of $p_\parallel = m_e c\mathbf{a}_i^2/2$ [27–29].

In the LP case, strong-field ionization dominantly occurs at the crests of the electric field, which leads to vanishing residual energy and momentum because $\mathbf{a}_i = 0$. Energy and momentum gain is only possible for a phase mismatch ϕ_0 which is suppressed due to the exponential dependence of the ADK ionization rates with electric field strength [43, 44].

For CP pulses the amplitude of the electric field follows the pulse envelope and the vector potential $\mathbf{a}$ is 90 degrees out of phase with $\mathbf{E}$, but its magnitude at the moment of ionization a_i is non-vanishing. Because of this, the ATI momentum and energy are significantly larger for CP pulses compared to LP.

In a wakefield bubble, electrons originate from a narrow cylindrical collection volume located $\sim \lambda_p$ from the beam axis and flow along the bubble sheath. At the back of the blowout region, if their forward velocity v_z exceeds the wake phase velocity v_p they can be trapped and accelerated by the plasma wakefields. The small initial transverse momentum from ATI can slightly alter the trajectories of electrons around the bubble sheath and introduce an asymmetry to these orbits. Some electrons, which start at the correct azimuthal angle where the laser vector potential points inward, will be trapped more easily. In Fig. 4 (b) the electron orbits from particle tracking simulations show this asymmetry in otherwise symmetric plasma fields.

Helium as target medium works well for this study because to field-ionize He^+ to He^{2+} (IP $E_{\rm ion} = 54.54$ eV), the required field strength is relatively high, yielding a large ATI momentum. It can be estimated using the barrier suppression ionization (BSI) model [45], yielding for CP $I_{\rm BSI}[{\rm W/cm^2}] = 8{\times}10^9\, E_{\rm ion}^4[{\rm eV}]/Z^2 = 1.8{\times}10^{16}$. This corresponds to $a_i \simeq 0.064$, which in turn gives the value of ATI momentum $p_\perp \simeq 33$ keV/c and $p_\parallel \simeq 1$ keV/c $\ll p_\perp$. And because of $p_\parallel \ll p_\perp$ also $E_{\rm kin} \simeq m_e c^2\mathbf{a}_i^2/2$. For LP the BSI estimate gives $p_\perp \sim p_\parallel \sim 0$.

A 1D PIC simulation including ADK ionization model using the EPOCH code [46] also confirmed the theoretical hypothesis. Fig. 3(a) illustrates the clear difference

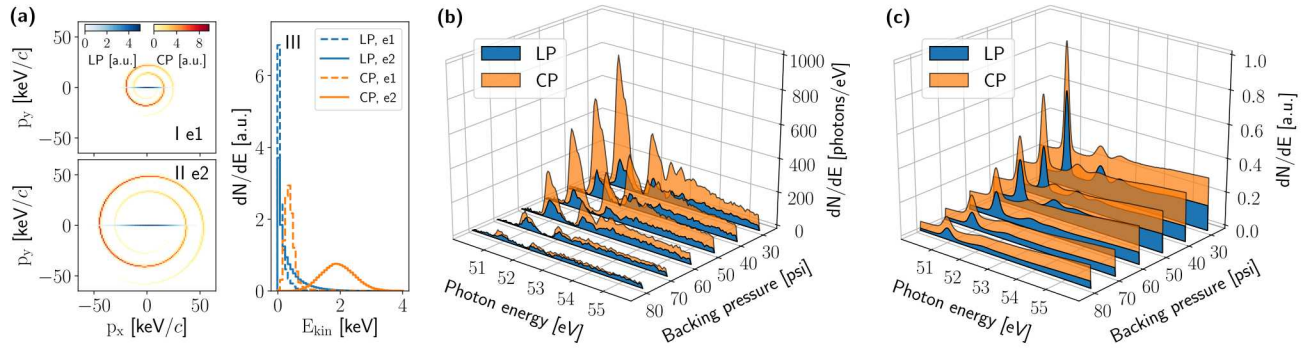

FIG. 3. (a) Electron momenta gain (I, II) and kinetic energy gain (III) in EPOCH simulations. A diluted plasma with a density of $1 \times 10^6 \mathrm{cm}^{-3}$ was used in these simulations to mitigate plasma effects which allows to highlight the differences in ionization between LP (blue) and CP (orange). The peak laser intensity in these simulations is fixed at 1×10^{18} W/cm^2. (b) Experimentally measured XUV photon spectra for various Helium backing pressures (i.e. plasma densities). (c) XUV spectra from SCRAM [41] atomic physics simulations with a thermal electron energy distribution with the same average energies as the electron spectra from (a) III.

of transverse and longitudinal momenta of the two Helium electrons due to field ionization. For the LP laser, the transverse momentum is mainly along the polarization direction. For the CP laser there is a clear spiral structure, due to the ramp-up of the laser pulse envelope, in the transverse phase space of (p_x, p_y), which indicates much larger momentum gain. This also results in a much larger longitudinal momentum gain for CP than LP. Note that for the CP laser, the momentum gain is mainly contributed by the second ionization level.

Employing a static wake approximation, the Hamiltonian $H = \gamma(1 - \beta_p\beta_z) - \Psi$, where $\Psi = \frac{e}{mc^2}(\Phi - \beta_p A_z)$ is the (normalized) wake potential, is a constant [47–49]. For a cold plasma this constant value is $H_i = 1$ because $\Psi_i = 0$. For such quiescent electrons trapping occurs mainly due to bubble evolution [50], i.e. nonstatic wakefield effects. In ionization injection schemes trapping is enabled by electrons from deeply bound states (e.g. the 1s electrons of nitrogen) that are ionized close to the *peak* of the laser pulse where $\Psi_i = \mathcal{O}(1)$ is large [49], lowering the value of H significantly. Here, the ionization of He happens at the front of the laser pulse where the $\Psi_i \ll 1$ and the value of $H_i \approx 1$. This clearly shows that the mechanism discussed in this letter is very distinct from ionization injection, despite the fact that it involves ionization dynamics.

The difference of the residual momenta and hence kinetic energies with different laser polarization will eventually lead to higher plasma temperatures for CP [51, 52]. In our experiment, this was confirmed by measurements of the time-integrated XUV spectra as shown in Fig. 3(b) and atomic physics simulations with the code SCRAM [41]. The SCRAM calculations, shown in Fig. 3(c), used a thermal plasma that was allowed to cool by radiative emission, with initial temperature corresponding to the same average energy per electron as the LP and CP distributions. In Fig. 3(b), there is increased emission in the CP case compared with the LP case, consistent with the increased temperature. The decrease of measured emission as the gas pressure increases is probably due to the opacity of the $\sim$ cm scale gas medium.

Consequently, circular polarization leads to significant differences in self-injection because it modifies the initial conditions for the electron trajectories and trapping is extremely sensitive to the details of the trajectory. To further investigate the effect of the ionization dynamics on electron trajectories, we examined the initial position of the trapped electrons in three-dimensional space in the co-moving frame for both LP and CP cases, as shown in Fig. 4(a). In the CP case, one can clearly see that trapped electrons originate from a spiral structure at the evolving ionization front and the projection in the transverse plane is a ring with a width of approximately 1 μm. In the LP case, the trapped electrons originate from the vicinity of only two particular angles in the polarization plane. The spiral structure in CP case is due to the fact that the transverse vector potential at ionization induces an asymmetry to the electron orbits that follow the bubble sheath. As the vector potential rotates, the spiral structure forms. This feature was confirmed by particle tracking using static fields obtained from the PIC simulations, as shown in Fig. 4(b). One can see that at a certain time, the initial positions of the trapped electrons are all located within a small azimuthal angle where the vector potential points towards the axial axis.

In conclusion, we have investigated the effect of laser polarization on self-injection in LWFA in both experiments and numerical simulations. Our experimental results demonstrate that with a CP laser, the injection threshold can be much lower than that with an LP laser. Theoretical analysis and numerical simulations revealed the important role of polarization-dependent above threshold ionization dynamics in facilitating self-injection.

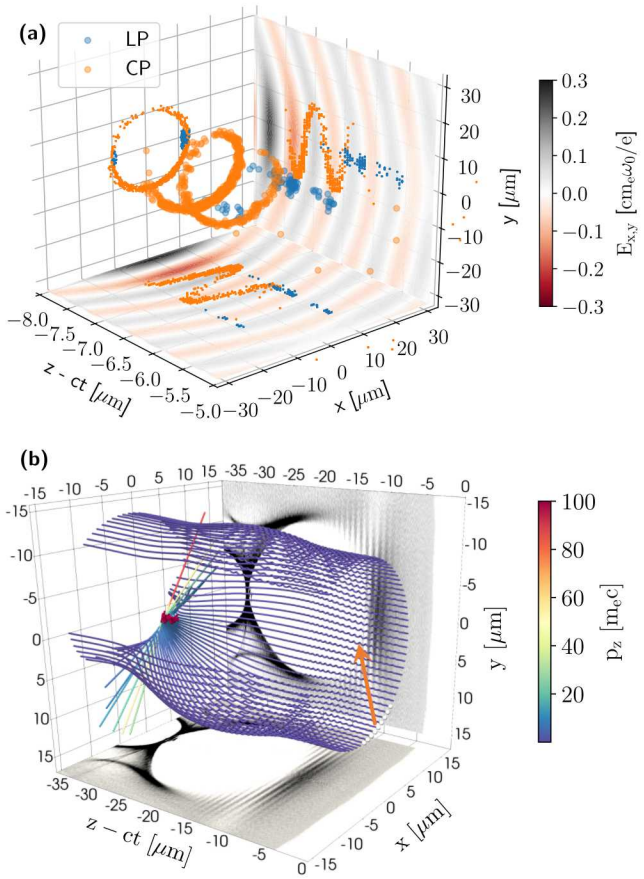

FIG. 4. (a) Initial position of injected electrons at born in the co-moving frame. For CP laser, electrons born at any phase in the ionization front, which is about 1 wavelength, can be injected. For LP laser, only those born in the polarization plane at $\phi_0 = 0$ or π can be injected. Note that the angular distribution of the electrons in CP is not perfectly cylindrical symmetric. This is because that the field strength is not constant during the ionization which results in a balance between high field strength and ionization degree. (b) Particle tracking with static fields from PIC simulation in the CP laser case. The white dots represent the initial positions for the trapped particles. The orange arrow represents the direction of the vector potential at the starting point of the trajectories.

The method demonstrated here is fundamentally different from ionization injection reported in the literature, where injected electrons from the inner shell of mid-Z materials (such as Nitrogen and Oxygen) are born inside the bubble, close to the peak laser intensity [49, 53]).

Our method is not limited to low-Z material, such as Helium. It can perform even better with mid-Z materials to take advantage of the various ionization potentials for various ionization levels. For example, the IP for the third to sixth electrons of Oxygen lies in between the IP of the second electron of Helium and the sixth electron of Nitrogen. Ionization of these electrons doesn't need the high laser intensity required by ionization injection, but can give momenta gain higher than that of the second electron of Helium.

This work was supported by DOE Office of Science, Fusion Energy Sciences under Contract No. DE-SC0019255: the LaserNetUS initiative at the Gérard Mourou Center for Ultrafast Optical Sciences and Grant DE-SC0019186. SNL is managed and operated by NTESS under DOE NNSA contract DE-NA0003525. The work of SH was supported by U.S. Department of Energy, Office of Science Early Career Research Program, Office of Fusion Energy Sciences under FWP-14-017426 and Sandia National Laboratories, a multimission laboratory managed and operated by NTESS, LLC., a wholly owned subsidiary of Honeywell International, Inc., for the U.S. DOE's NNSA under contract DE-NA-0003525. This research was supported in part through computational resources and services provided by Advanced Research Computing at the University of Michigan, Ann Arbor.

* yongm@umich.edu

[1] T. Tajima and J. M. Dawson, Phys. Rev. Lett. **43**, 267 (1979).
[2] A. J. Gonsalves, K. Nakamura, J. Daniels, C. Benedetti, C. Pieronek, T. C. H. de Raadt, S. Steinke, J. H. Bin, S. S. Bulanov, J. van Tilborg, C. G. R. Geddes, C. B. Schroeder, C. Tóth, E. Esarey, K. Swanson, L. Fan-Chiang, G. Bagdasarov, N. Bobrova, V. Gasilov, G. Korn, P. Sasorov, and W. P. Leemans, Phys. Rev. Lett. **122**, 084801 (2019).
[3] W. P. Leemans, A. J. Gonsalves, H.-S. Mao, K. Nakamura, C. Benedetti, C. B. Schroeder, C. Tóth, J. Daniels, D. E. Mittelberger, S. S. Bulanov, J.-L. Vay, C. G. R. Geddes, and E. Esarey, Phys. Rev. Lett. **113**, 245002 (2014).
[4] H. T. Kim, K. H. Pae, H. J. Cha, I. J. Kim, T. J. Yu, J. H. Sung, S. K. Lee, T. M. Jeong, and J. Lee, Phys. Rev. Lett. **111**, 165002 (2013).
[5] X. Wang, R. Zgadzaj, N. Fazel, Z. Li, S. A. Yi, X. Zhang, W. Henderson, Y. Y. Chang, R. Korzekwa, H. E. Tsai, C. H. Pai, H. Quevedo, G. Dyer, E. Gaul, M. Martinez, A. C. Bernstein, T. Borger, M. Spinks, M. Donovan, V. Khudik, G. Shvets, T. Ditmire, and M. C. Downer, Nature Communications **4**, 1988 (2013).
[6] G. Sarri, W. Schumaker, A. Di Piazza, M. Vargas, B. Dromey, M. E. Dieckmann, V. Chvykov, A. Maksimchuk, V. Yanovsky, Z. H. He, B. X. Hou, J. A. Nees, A. G. R. Thomas, C. H. Keitel, M. Zepf, and K. Krushelnick, Phys. Rev. Lett. **110**, 255002 (2013).
[7] S. Kneip, C. McGuffey, J. L. Martins, S. F. Martins, C. Bellei, V. Chvykov, F. Dollar, R. Fonseca, C. Huntington, G. Kalintchenko, A. Maksimchuk, S. P. D. Mangles, T. Matsuoka, S. R. Nagel, C. A. J. Palmer, J. Schreiber, K. T. Phuoc, A. G. R. Thomas, V. Yanovsky, L. O. Silva, K. Krushelnick, and Z. Najmudin, Nature Physics **6**, 980 (2010).
[8] W. Yan, C. Fruhling, G. Golovin, D. Haden, J. Luo, P. Zhang, B. Zhao, J. Zhang, C. Liu, M. Chen, S. Chen, S. Banerjee, and D. Umstadter, Nat. Photonics **11**, 514

(2017).
[9] G. Sarri, D. J. Corvan, W. Schumaker, J. M. Cole, A. Di Piazza, H. Ahmed, C. Harvey, C. H. Keitel, K. Krushelnick, S. P. D. Mangles, Z. Najmudin, D. Symes, A. G. R. Thomas, M. Yeung, Z. Zhao, and M. Zepf, Phys. Rev. Lett. **113**, 224801 (2014).
[10] J. M. Cole, K. T. Behm, E. Gerstmayr, T. G. Blackburn, J. C. Wood, C. D. Baird, M. J. Duff, C. Harvey, A. Ilderton, A. S. Joglekar, K. Krushelnick, S. Kuschel, M. Marklund, P. McKenna, C. D. Murphy, K. Poder, C. P. Ridgers, G. M. Samarin, G. Sarri, D. R. Symes, A. G. R. Thomas, J. Warwick, M. Zepf, Z. Najmudin, and S. P. D. Mangles, Phys. Rev. X **8**, 011020 (2018).
[11] K. Poder, M. Tamburini, G. Sarri, A. Di Piazza, S. Kuschel, C. D. Baird, K. Behm, S. Bohlen, J. M. Cole, D. J. Corvan, M. Duff, E. Gerstmayr, C. H. Keitel, K. Krushelnick, S. P. D. Mangles, P. McKenna, C. D. Murphy, Z. Najmudin, C. P. Ridgers, G. M. Samarin, D. R. Symes, A. G. R. Thomas, J. Warwick, and M. Zepf, Phys. Rev. X **8**, 031004 (2018).
[12] S. Corde, K. Ta Phuoc, G. Lambert, R. Fitour, V. Malka, A. Rousse, A. Beck, and E. Lefebvre, Rev. Mod. Phys. **85**, 1 (2013).
[13] F. Grüner, S. Becker, U. Schramm, T. Eichner, M. Fuchs, R. Weingartner, D. Habs, J. Meyer-ter Vehn, M. Geissler, M. Ferrario, L. Serafini, B. van der Geer, H. Backe, W. Lauth, and S. Reiche, Applied Physics B **86**, 431 (2007).
[14] A. Bernhard, V. A. Rodrguez, S. Kuschel, M. Leier, P. Peiffer, A. Svert, M. Schwab, W. Werner, C. Widmann, A. Will, A.-S. Mller, and M. Kaluza, Nuclear Instruments and Methods in Physics Research Section A: Accelerators, Spectrometers, Detectors and Associated Equipment **909**, 391 (2018), 3rd European Advanced Accelerator Concepts workshop (EAAC2017).
[15] A. Pukhov and J. Meyer-ter Vehn, Applied Physics B **74**, 355 (2002).
[16] W. Lu, M. Tzoufras, C. Joshi, F. S. Tsung, W. B. Mori, J. Vieira, R. A. Fonseca, and L. O. Silva, Phys. Rev. ST Accel. Beams **10**, 061301 (2007).
[17] D. Umstadter, J. K. Kim, and E. Dodd, Phys. Rev. Lett. **76**, 2073 (1996).
[18] E. Esarey, R. F. Hubbard, W. P. Leemans, A. Ting, and P. Sprangle, Phys. Rev. Lett. **79**, 2682 (1997).
[19] G. Fubiani, E. Esarey, C. B. Schroeder, and W. P. Leemans, Phys. Rev. E **70**, 016402 (2004).
[20] H. Kotaki, S. Masuda, M. Kando, J. K. Koga, and K. Nakajima, Physics of Plasmas **11**, 3296 (2004), https://doi.org/10.1063/1.1751171.
[21] M. Chen, Z. M. Sheng, Y. Y. Ma, and J. Zhang, Journal of Applied Physics **99**, 1 (2006).
[22] S. Bulanov, N. Naumova, F. Pegoraro, and J. Sakai, Phys. Rev. E **58**, R5257 (1998).
[23] L.-L. Yu, E. Esarey, C. B. Schroeder, J.-L. Vay, C. Benedetti, C. G. R. Geddes, M. Chen, and W. P. Leemans, Phys. Rev. Lett. **112**, 125001 (2014).
[24] C. Benedetti, C. B. Schroeder, E. Esarey, F. Rossi, and W. P. Leemans, Physics of Plasmas **20**, 103108 (2013), https://doi.org/10.1063/1.4824811.
[25] E. Esarey, C. B. Schroeder, E. Cormier-Michel, B. A. Shadwick, C. G. Geddes, and W. P. Leemans, Physics of Plasmas **14** (2007), 10.1063/1.2714022.
[26] E. Esarey, B. Hafizi, R. Hubbard, and A. Ting, Phys. Rev. Lett. **80**, 5552 (1998).
[27] C. I. Moore, A. Ting, S. J. McNaught, J. Qiu, H. R. Burris, and P. Sprangle, Phys. Rev. Lett. **82**, 1688 (1999).
[28] C. I. Moore, A. Ting, T. Jones, E. Briscoe, B. Hafizi, R. F. Hubbard, and P. Sprangle, Physics of Plasmas **8**, 2481 (2001), https://doi.org/10.1063/1.1347033.
[29] B. Zhou, A. Houard, Y. Liu, B. Prade, A. Mysyrowicz, A. Couairon, P. Mora, C. Smeenk, L. Arissian, and P. Corkum, Phys. Rev. Lett. **106**, 255002 (2011).
[30] T. Z. Zhao, K. Behm, C. F. Dong, X. Davoine, S. Y. Kalmykov, V. Petrov, V. Chvykov, P. Cummings, B. Hou, A. Maksimchuk, J. A. Nees, V. Yanovsky, A. G. R. Thomas, and K. Krushelnick, Phys. Rev. Lett. **117**, 094801 (2016).
[31] M. Vargas, W. Schumaker, Z.-H. He, Z. Zhao, K. Behm, V. Chvykov, B. Hou, K. Krushelnick, A. Maksimchuk, V. Yanovsky, and A. G. R. Thomas, Applied Physics Letters **104**, 174103 (2014), https://doi.org/10.1063/1.4874981.
[32] S. Kuschel, M. B. Schwab, M. Yeung, D. Hollatz, A. Seidel, W. Ziegler, A. Sävert, M. C. Kaluza, and M. Zepf, Phys. Rev. Lett. **121**, 154801 (2018).
[33] S. P. D. Mangles, *Measurements of Relativistic Electrons from Intense Laser-Plasma Interactions*, PhD dissertation, Imperial College London (2005).
[34] N. Nakanii, K. Kondo, T. Yabuuchi, K. Tsuji, K. A. Tanaka, S. Suzuki, T. Asaka, K. Yanagida, H. Hanaki, T. Kobayashi, K. Makino, T. Yamane, S. Miyamoto, and K. Horikawa, Review of Scientific Instruments **79**, 066102 (2008), https://doi.org/10.1063/1.2940217.
[35] Z. Zhao, *Control of Synchrotron X-ray Emission from Laser Wakefield Accelerators*, PhD dissertation, University of Michigan (2016).
[36] D. Neely, D. Chambers, C. Danson, P. Norreys, S. Preston, F. Quinn, M. Roper, J. Wark, and M. Zepf, in *Superstrong Fields in Plasmas*, AIP Conf. Proc. No. 426, edited by M. Lontano, G. Mourou, F. Pegoraro, and E. Sindoni (AIP, New York, 1998) pp. 479–484.
[37] P. Sprangle, C. Tang, and E. Esarey, IEEE Transactions on Plasma Science **15**, 145 (1987).
[38] A. J. Goers, G. A. Hine, L. Feder, B. Miao, F. Salehi, J. K. Wahlstrand, and H. M. Milchberg, Phys. Rev. Lett. **115**, 194802 (2015).
[39] S. P. D. Mangles, G. Genoud, M. S. Bloom, M. Burza, Z. Najmudin, A. Persson, K. Svensson, A. G. R. Thomas, and C.-G. Wahlström, Phys. Rev. ST Accel. Beams **15**, 011302 (2012).
[40] D. H. Froula, C. E. Clayton, T. Döppner, K. A. Marsh, C. P. J. Barty, L. Divol, R. A. Fonseca, S. H. Glenzer, C. Joshi, W. Lu, S. F. Martins, P. Michel, W. B. Mori, J. P. Palastro, B. B. Pollock, A. Pak, J. E. Ralph, J. S. Ross, C. W. Siders, L. O. Silva, and T. Wang, Phys. Rev. Lett. **103**, 215006 (2009).
[41] S. Hansen, J. Bauche, C. Bauche-Arnoult, and M. Gu, High Energy Density Physics **3**, 109 (2007).
[42] R. Lehe, M. Kirchen, I. A. Andriyash, B. B. Godfrey, and J.-L. Vay, Computer Physics Communications **203**, 66 (2016).
[43] P. B. Corkum, N. H. Burnett, and F. Brunel, Phys. Rev. Lett. **62**, 1259 (1989).
[44] M. V. Ammosov, N. B. Delone, and V. P. Krainov, Sov. Phys. JETP **64**, 1191 (1986).
[45] S. Augst, D. Strickland, D. D. Meyerhofer, S. L. Chin, and J. H. Eberly, Phys. Rev. Lett. **63**, 2212 (1989).
[46] T. D. Arber, K. Bennett, C. S. Brady, A. Lawrence-

Douglas, M. G. Ramsay, N. J. Sircombe, P. Gillies, R. G. Evans, H. Schmitz, A. R. Bell, and C. P. Ridgers, Plasma Physics and Controlled Fusion **57**, 1 (2015).
[47] E. Esarey and M. Pilloff, Phys. Plasmas **2**, 1432 (1995).
[48] W. Lu, C. Huang, M. Zhou, M. Tzoufras, F. S. Tsung, W. B. Mori, and T. Katsouleas, Phys. Plasmas **13**, 056709 (2006).
[49] A. Pak, K. A. Marsh, S. F. Martins, W. Lu, W. B. Mori, and C. Joshi, Phys. Rev. Lett. **104**, 025003 (2010).
[50] S. Y. Kalmykov, S. A. Yi, A. Beck, A. F. Lifschitz, X. Davoine, E. Lefebvre, A. Pukhov, V. Khudik, G. Shvets, S. A. Reed, P. Dong, X. Wang, D. Du, S. Bedacht, R. Zgadzaj, W. Henderson, A. Bernstein, G. Dyer, M. Martinez, E. Gaul, T. Ditmire, and M. C. Downer, New J. Phys. **12** (2010), 10.1088/1367-2630/12/4/045019.
[51] B. M. Penetrante and J. N. Bardsley, Phys. Rev. A **43**, 3100 (1991).
[52] N. Lemos, T. Grismayer, L. Cardoso, J. Geada, G. Figueira, and J. M. Dias, Phys. Plasmas **20**, 103109 (2013).
[53] C. McGuffey, A. G. R. Thomas, W. Schumaker, T. Matsuoka, V. Chvykov, F. J. Dollar, G. Kalintchenko, V. Yanovsky, A. Maksimchuk, K. Krushelnick, V. Y. Bychenkov, I. V. Glazyrin, and A. V. Karpeev, Phys. Rev. Lett. **104**, 025004 (2010).